

Effectiveness of Nanosilver, Nanogold and their Combination on the Healing Potential of Critical Radial Bone Defects in Rats

Ahmad Oryan¹, Hojjat Gholipour² and Abdolhamid Meimandi-Parizi^{2*}

¹Department of Pathology, School of Veterinary Medicine, Shiraz University, Shiraz, Iran

²Division of Surgery, Department of Clinical Sciences, School of Veterinary Medicine, Shiraz University, Shiraz, Iran

Abstract

A new composition of platelet-fibrin glue (FPG), gelatin (Gel), nanohydroxyapatite (nHA), silver nanoparticles (SNPs) and gold nanoparticles (GNPs) was synthesized and employed in preparation of hybrid scaffolds and was applied in bone tissue engineering in the surgically critical-sized bone defect in a rat model. Sixty bilateral radial bone defects were randomly divided into six groups including untreated defects, autograft and those treated with Gel/FPG/nHA containing scaffolds including nHA alone, nHA/SNPs, nHA/GNPs and nHA/SNPs/GNPs (n=10 in each group). The defects were assessed by radiography, histopathology, scanning electron microscopy and biomechanical testing. In comparison with the untreated defects, all the treated defects demonstrated significantly superior new bone formation, remodeling and bone tissue volume. Moreover, the defects treated with GNPs showed significantly higher ultimate strength, yield strength and stiffness. The nHA and nHA/SNPs moderately improved bone regeneration that were not close to the autograft in some parameters, whereas nHA/GNPs and nHA/SNPs/GNPs significantly improved bone healing closely comparable with those of the autograft group in most parameters. In conclusion, although all the scaffolds had some beneficial effectiveness on bone regeneration, the scaffolds containing GNPs were more effective in improving the structural and functional properties of the newly formed bone and were more osteoinductive than other scaffolds and were comparable to the autograft. Therefore, the scaffolds including GNPs can be regarded as a promising option to be used in bone tissue engineering.

Keywords: Nanogold; Nanosilver; Nanohydroxyapatite; Radius; Bone healing; Rat

Introduction

Natural polymers and calcium phosphate composites are the widely used biomaterials in bone tissue engineering [1]. Among them, nanohydroxyapatite (nHA) is chemical analogue of the mineral component of bone and has been extensively investigated in various forms and shapes as a perfect inorganic component of synthetic materials in orthopedics and bone tissue engineering for decades [1-3]. Nano-sized HA particles increase protein adsorption and cell adhesion to internal surfaces of the scaffold and improve the mechanical and biological properties [1,4,5]. Nonetheless, the brittleness, poor mechanical properties and low flexural strength of nHA renders it unsuitable as a composite material used alone in regeneration of different parts of the bone systems, especially those under significant mechanical tension [2,6]. To overcome such limitations, a number of HA-based composite materials, using both natural and synthetic polymers, have been developed [2,3]. Polymers combined with HA can enhance the formation of new bone tissue by promoting osteoblast adhesion, migration, differentiation and proliferation, and deposition of calcium containing minerals on its surface [1,6]. Based on the current condition of bone tissue engineering, fibrin-platelet glue (FPG) and Gelatin (Gel) have wide tissue engineering applications so that they are used as the basic biomaterials in manufacturing of various bone scaffolds. These are both applied in combination with other polymeric and ceramic materials in order to fabricate composite bone scaffolds [6,7].

As far as orthopedic implants such as the HA-based scaffold are considered, bacterial infection is a predicament issue and bacterial resistance may increase the risk of infections leading to implant failure, hospitalization and sometimes to mortality of the patient [1,8,9]. Metal nanoparticles such as copper, zinc, silver and gold have antimicrobial properties [1]. The broad-spectrum antimicrobial features of silver are defined against some of the potential harmful pathogenic microorganisms and it has been applied in different fields in medicine

since years [9]. Many studies showed this antimicrobial activity towards bone implant and bone regenerative medicine [1,10,11]. Silver also affects physicochemical features of the scaffolds, like gel fraction, porosity, swelling behavior, and morphology [10]. Cytotoxicity of composite loaded with silver salts made this type of silver inappropriate for all day clinical application in the past. The new nanoparticle form of silver (SNPs) is free of cytotoxicity, *in vitro* and has shown high effectiveness against multi-resistant bacteria [9].

Developments of nanotechnology in the recent decades resulted in application of gold nanoparticles (GNPs) towards drug delivery, cell targeting, biosensing and tissue engineering [12-14]. GNPs are a new generation of osteogenic agents in bone tissue regeneration and the GNPs multicomponent composites could find numerous applications in bone tissue engineering, given the great biocompatibility, low cytotoxicity, 3D structure, and unique composition [2,12]. GNPs exhibit a positive consequence on the osteogenic differentiation of mesenchymal stem cells (MSCs) and osteoblast-like cells and induce excellent bone cellular proliferation [15,16]. The nHA/GNPs has tremendous potential to be applied as multicomponent materials in bone regeneration, especially given that HA is a natural bone component and the gold nanoparticles have low cytotoxicity [2].

***Corresponding author:** Abdolhamid Meimandi-Parizi, Division of Surgery, Department of Clinical Sciences, School of Veterinary Medicine, Shiraz University, Shiraz, Iran, Tel: (+98) 917 111 2934; Fax: (+98) 713 228 6940; E-mail: meimandi@shirazu.ac.ir

Received December 05, 2017; **Accepted** January 30, 2018; **Published** February 05, 2018

Citation: Oryan A, Gholipour H, Meimandi-Parizi A (2018) Effectiveness of Nanosilver, Nanogold and their Combination on the Healing Potential of Critical Radial Bone Defects in Rats. J Tissue Sci Eng 9: 215. doi: [10.4172/2157-7552.1000215](https://doi.org/10.4172/2157-7552.1000215)

Copyright: © 2018 Oryan A, et al. This is an open-access article distributed under the terms of the Creative Commons Attribution License, which permits unrestricted use, distribution, and reproduction in any medium, provided the original author and source are credited.

This work presents the very first attempt in making a hybrid FPG/Gel/nHA/SNPs and GNPs scaffold to be used in bone tissue engineering in the surgically critical-sized radial bone defect (CSD) in a rat model. Such a hybrid structure combines the beneficial properties of the Gel, FPG, nHA, SNPs and GNPs. Embedment of the nanoparticles into the FPG/Gel/nHA may be an excellent technique to improve the functionality of the composite scaffold. Such a composite scaffold with both polymeric and nano-sized materials also provides a proper surface harshness and appropriate mechanical strength, which may enhance bone tissue regeneration [12,17]. We studied the effects of incorporation of SNPs and GNPs in the scaffold. We hypothesized that both the SNPs and GNPs may have some useful effects on bone regeneration but each of such nanoparticles may have different potency. In addition, combination of these nanoparticles may keep the useful effects of both nanoparticles, while this strategy may reduce the limitations of the individuals.

Materials and Methods

Ethics

The animals received humane care according to the Guide for the Care and Use of Laboratory Animals published by the National Institutes of Health (NIH) [18]. The study was authorized by the local Ethics Committee of "Regulations for Using Animals in Scientific Procedures" in our school of veterinary medicine.

Preparation of the scaffolds

The Gel/nHA, Gel/nHA/SNPs, Gel/nHA/GNPs and Gel/nHA/SNPs/GNPs scaffolds were first prepared by chemical cross-linking of gelatin (G9391, Sigma-Aldrich). Gelatin cross linking was performed using glutaraldehyde (G6403, Sigma-Aldrich), in presence of medical-grade nano-hydroxyapatite granules of the mean size of 30 nm (Pardis Pajooheh Fanavarani Co., Yazd, Iran), silver nanoparticles (US Research Nanomaterials Inc., Houston, USA) and gold nanoparticles (US Research Nanomaterials Inc., Houston, USA). Then, we introduced fibrin-platelet glue into the porous scaffolds to fabricate the FPG-containing hybrid scaffolds. Briefly, 4.29 wt% aqueous solution of gelatin at 20% volume weight of nHA (7 ml) was mixed at 5000 rpm at 37°C for 3 min, using a homogenizer (Sealed Unit, Silverson Machines Ltd., UK). For the SNPs and GNPs containing scaffolds, nHA was loaded with 1% weight ratio of SNPs and GNPs. After addition of the glutaraldehyde aqueous solution, the resulting solution was cast into a polypropylene dish at 4°C for 12 h for cross-linking. The cross-linked scaffolds were then placed into 100 mM aqueous glycine solution at 37°C for 1 h to block the residual aldehyde groups of glutaraldehyde. Following complete washing with double distilled water, the scaffolds were freeze-dried at -20°C for 48 h (Alpha 2-4 LD Plus, Christ, Germany). The scaffolds were finally sterilized under 60 Co γ -ray irradiation at a dose of 15 kGy and kept in vacuumed packs until further use [6,19].

The FPG was prepared from the platelet rich plasma (PRP) of rat by the Thorn et al. method [20]. Briefly, the blood was collected via heart aspiration and mixed with citrate phosphate dextrose at a ratio of 1 ml citrate phosphate dextrose to 5 ml blood. The PRP was separated from the blood by centrifugation (IEC PR-J centrifuge, Damon/IEC Division, USA) for 15 min at 327x g. The fibrinogen in the glue was precipitated from the PRP by ethanol precipitation at low temperature. The precipitated fibrinogen was separated by centrifugation at 3000x g for 8 min at 0-4°C. The separated fibrinogen together with the modified PRP was used to enrich the fibrinogen with growth factors. Thorn et al. [20] reported that the autologous fibrin glue prepared by this technique contains high platelet and fibrinogen concentrations.

The hybrid FPG-containing scaffolds were prepared as follows: The Gel/nHA, Gel/nHA/SNPs, Gel/nHA/GNPs and Gel/nHA/SNPs/GNPs scaffolds, sterilized previously with 60 Co γ -ray irradiation, were infused with 0.1 ml platelet enriched fibrinogen solution for 5 min, then with 0.1 ml calcium chloride (Merck, Cat. No. 102382)/topical bovine thrombin (T-4648, Sigma-Aldrich) (10 CC of 10% calcium chloride mixed with 10,000 units of topical bovine thrombin) for preparation of FPG [21,22]. After complete reaction for 30 min at room temperature, the hybrid scaffolds were freeze-dried at -20°C for 48 h and kept in vacuumed packs until further use [6].

Animals and operative procedures

A total of 30 mature male Wistar Albino rats, weighing between 250 to 300 g, purchased from Shiraz University of Medical Sciences, Shiraz, Iran, were used in this study. The animals had full access to standard food and water ad libitum throughout the duration of the study. The rats were anesthetized with an intramuscular injection, using a combination of 75 mg/kg ketamine and 5 mg/kg xylazine (both from Alfasan; Woerden, Netherlands). The right and left forelimbs of all the animals were prepared aseptically for operation. An incision was made craniomedially over the skin of each forelimb and the radius was exposed by dissecting the surrounding muscles and tendons. A 5 mm segmental bone defect was created in the middle of the radial diaphysis as a critical size bone defect by an electrical bone saw at 150 rpm under saline irrigation to prevent thermal necrosis (Marathon, Escort-III, Daegu, South Korea). All bone debris and interosseous membrane in the defect site were washed and wiped away.

As the radius and ulna are fused together by interosseous membrane, adequate stability was achieved by leaving the ulna intact without any fixation of the radius. A total of 60 radial bone defects were created in the 30 rats. The bone defects were randomly divided into six equal groups (n=10 in each group). The defects in the 1st group remained intact and served as negative control (-C group) for the test groups. The defects in the 2nd group were filled with autologous bone graft to be considered as positive control (+C group). In a group of animals containing both groups of -C (right side) and +C (left side), the autografts were harvested from the contralateral radii of the group 1 so that the transected corticomedullary bone segment in the empty defect group (right side) was used as autograft to fill the defect area of the group 2 (left side). The defects in the 3rd, 4th, 5th and 6th groups (test groups) were filled with Gel-FPG-nHA (nHA group), Gel-FPG-nHA-SNPs (SNPs group), Gel-FPG-nHA-GNPs (GNPs group) and Gel-FPG-nHA-SNPs-GNPs (SNPs+GNPs group), having the size and shape similar to the radial defects ($2 \times 2 \times 5 \text{ mm}^3$), respectively. The muscles, fascia and skin were then approximated in a routine fashion, using 4-0 sutures (Ethicon; Somerville, New Jersey, USA). Post-surgically, analgesia and antibiotic therapy were performed by daily sub-cutaneous injections of 20 mg/kg tramadol chloride (Darou Pakhsh Pharmaceutical Mfg. Co., Tehran, Iran) for 3 days and 20 mg/kg enrofloxacin (Razak Laboratory Co., Tehran, Iran) for 5 days.

Clinical examination

After surgery and induction of bone defects, the rats were observed for physical activities including weight bearing on injured forearms, and post-surgical clinical changes such as edema and hyperemia in the defect area, pain on palpation and the appetite status.

Radiological evaluation

To evaluate bone formation, proximal and distal union and remodeling of the defect, radiographs of each forelimb was taken postoperatively on the 1st day and then at the 28th and 56th days post

injury, using an X-ray machine (Soyee, BLD-31-C, Seoul, South Korea). The results were blindly scored, using the modified Lane and Sandhu scoring system by two veterinary radiologists [23,24] (Table 1).

Sample collection

Fifty-six days after operation the rats were euthanized [25,26]. For such purpose, first, the animals were anesthetized by intramuscular injection of ketamine and xylazine. The breathing of the anesthetized animals was then stopped by intracardiac injection of 150 mg/kg potassium chloride (Pasteur Institute, Tehran, Iran). The right and left forelimbs were harvested and dissected free of soft tissues. The bone samples of each group (n=10) were randomly divided into two equal subgroups as follow: Subgroup A (n=5): these bone samples were used for histopathologic and scanning electron microscopic studies (SEM). These bone samples were cut to two pieces with sagittal sections containing the defect for histopathologic and SEM studies. For this purpose, the bones were cut to two pieces containing the defect with a sagittal section made by a slow speed saw. Thus, the same tissue was investigated for both methods [histopathology (n=5) and SEM (n=5)]. The bone samples in subgroup B (n=5) were used for biomechanical testing.

Histopathological evaluation

The bone specimens were fixed in 10% neutral buffered formalin. The formalin-fixed bone samples were rinsed with water and then decalcified in 10% nitric acid solution and processed for routine histological examination. Next, two 5 µm thick sections were cut in a

longitudinal direction from the center of each specimen and stained with Hematoxylin and Eosin (H&E) for analysis by light microscopy (Olympus CX-41, Tokyo, Japan). Finally, the sections were blindly evaluated and scored by two pathologists according to Emery's scoring system [27,28] (Table 2). Images of the histologic sections were captured by a digital camera (Olympus E-P1, Olympus Optical, Tokyo, Japan) connected to a light microscope. The volumes of the regenerated fibrous, cartilage and bone tissues in defected area were also calculated from the provided images [19,29].

Scanning electron microscopy

To visualize the morphological characterization of the healing area, the bone specimens were fixed in cold 2.5% buffered glutaraldehyde. After dehydration with an increasing graded ethanol series, the samples were dried, using a freeze drier. The dried specimens were coated with a few nanometers layer of gold by sputtering (SPI-Module Sputter Coater) and were mounted on SEM aluminum stubs, using carbon double-sided tape. The coated samples were degassed in vacuum and observed, using high-resolution images obtained, using filed emission SEM (Vega-3, Tescan, AS, Brno, Czech Republic) with accelerating voltage of 20 kV at different magnifications.

Biomechanical testing

The bone samples were wrapped in a saline-soaked gauze bandage to prevent dehydration and stored at -20°C in small, sealed freezer bags. At the day of testing, the bones were slowly thawed to room temperature and kept wrapped in the saline-soaked gauzes except during measurements. Mechanical testing was performed on the fused radius and ulna complex as a unit. The three-point bending test was performed, using a universal tensile testing machine (Santam, STM-20, Tehran, Iran) to determine the mechanical properties of bones according to the previously described procedures [30-32]. Briefly, the bones were placed on their lateral surface on the two rounded supporting bars (plates with rounded edges of 4.0 mm diameter) located at a distance of 16 mm and were loaded at the midpoint of the diaphysis by lowering the third bar (a plate with rounded edges of 10 mm diameter) so that the defect was in the middle and had an equal distance from each grip. The bones were loaded at a rate of 1 mm/s until fracturing occurred. The behavior of each specimen under loading was characterized by determining the following parameters from the load-deformation to destruction curve:

1. Ultimate strength or maximum load was determined as the highest point of the load-deformation curve (N).
2. Yield strength was determined as the point in the stress-strain curve at which the curve levels off and plastic deformation begins to occur (N). Prior to the yield point the material will deform elastically and will return to its original shape when the applied stress is removed. Once the yield point is passed, some fraction of the deformation will be permanent and non-reversible.
3. Stiffness is the coefficient of inclination for the linear portion of the load-deformation curve. It is easily calculated by measuring the slope of a line drawn as a tangent to the curve at any defined point in the linear portion of the curve. The slope gives the approximate stiffness of the preparation (N/mm).
4. Strain is the specimen's extension (the percentage of elongation) at the ultimate strength region. The term "strain" means the fractional increase in length of the material due to an applied

Bone formation	
No evidence of bone formation	0
Bone formation occupying 25% of the defect	1
Bone formation occupying 50% of the defect	2
Bone formation occupying 75% of the defect	3
Bone formation occupying 100% of the defect	4
Union (proximal and distal parts were evaluated separately)	
No union	0
Possible union	1
Radiographic union	2
Remodeling	
No evidence of remodeling	0
Remodeling of medullary canal	1
Full remodeling of cortex	2
Total point possible per category	
Bone formation	4
Proximal union	2
Distal union	2
Remodeling	2
Maximum score	10

Table 1: Modified Lane and Sandhu radiological scoring system.

Score (points)	Tissue present
0	Empty
1	Fibrous tissue only
2	More fibrous tissue than fibrocartilage
3	More fibrocartilage than fibrous tissue
4	Fibrocartilage only
5	More fibrocartilage than bone
6	More bone than fibrocartilage
7	Bone only

Table 2: Emery's histopathological scoring system.

load. It is calculated by dividing the extension by the original length of the specimen.

- Energy absorption was determined as the area under the load-deformation curve until the point of failure (*N.mm*).

The data derived from the load deformation curves were expressed as Mean \pm SEM for each group and the ultimate and yield strength, stiffness, ultimate and yield strain and absorbed energy were measured and recorded.

Statistical analysis

The radiological and histopathological data were compared by Kruskal-Wallis; non-parametric analysis of variance (ANOVA); when the *P-values* were found to be less than 0.05, then pair wise group comparisons was performed by Mann-Whitney U test. The biomechanical data were compared by one-way ANOVA with subsequent Tukey post-hoc tests. A *P*<0.05 was considered statistically significant. All biomechanical

data passed normally distribution test and Bonferroni's method used for multiple testing and the results were presented as means \pm SEM (SPSS version 23 for windows, SPSS Inc., Chicago, USA).

Results

Clinical evaluation

No death occurred among the animals during the course of the experiment and they had good physical activities, weight gain and appetite until euthanasia. The animals in all the groups used their forearms because of the ulna and its supportive role.

Radiological findings

The results of radiological evaluations at 28th and 56th days after bone surgery are presented in Table 3 and Figure 1. The -C group showed significantly the lowest bone formation, remodeling and

		Postoperative Days	Mean \pm SD Median (min-max)					
			Control		Treatment			
			-C (n=10)	+C (n=10)	nHA (n=10)	SNPs (n=10)	GNPs (n=10)	SNPs+GNPs (n=10)
Bone Formation		28	1.08 \pm 0.29 1 (1-2) ^a	2.64 \pm 0.50 3 (2-3) ^b	1.92 \pm 0.52 2 (1-3) ^c	2.25 \pm 0.45 2 (2-3) ^{bc}	2.77 \pm 0.60 3 (2-4) ^b	2.69 \pm 0.63 3 (2-4) ^{bc}
		56	1.36 \pm 0.67 1 (1-3) ^a	3.18 \pm 0.75 3 (2-4) ^b	2.73 \pm 0.65 3 (2-4) ^b	3.09 \pm 0.70 3 (2-4) ^b	3.15 \pm 0.69 3 (2-4) ^b	3.15 \pm 0.69 3 (2-4) ^b
Union	Proximal	28	0.67 \pm 0.49 1 (0-1) ^a	1.55 \pm 0.52 2 (1-2) ^b	0.92 \pm 0.29 1 (0-1) ^a	0.92 \pm 0.29 1 (0-1) ^a	1.15 \pm 0.38 1 (1-2) ^{ab}	1.15 \pm 0.38 1 (1-2) ^{ab}
		56	1.00 \pm 0.45 1 (0-2) ^a	1.73 \pm 0.47 2 (1-2) ^b	1.36 \pm 0.50 1 (1-2) ^{ab}	1.18 \pm 0.41 1 (1-2) ^a	1.46 \pm 0.52 1 (1-2) ^{ab}	1.39 \pm 0.51 1 (1-2) ^{ab}
	Distal	28	0.33 \pm 0.49 0 (0-1) ^a	1.45 \pm 0.52 1 (1-2) ^b	1.17 \pm 0.39 1 (1-2) ^b	1.17 \pm 0.39 1 (1-2) ^b	1.23 \pm 0.44 1 (1-2) ^b	1.23 \pm 0.44 1 (1-2) ^b
		56	0.82 \pm 0.75 1 (0-2) ^a	1.81 \pm 0.40 2 (1-2) ^b	1.36 \pm 0.50 1 (1-2) ^{ab}	1.45 \pm 0.52 1 (1-2) ^{ab}	1.69 \pm 0.68 2 (1-2) ^b	1.62 \pm 0.51 2 (1-2) ^b
Remodeling		28	0.08 \pm 0.29 0 (0-1) ^a	1.00 \pm 0.00 1 (1-1) ^b	1.08 \pm 0.28 1 (1-2) ^b			
		56	0.09 \pm 0.30 0 (0-1) ^a	1.09 \pm 0.30 1 (1-2) ^b	1.09 \pm 0.30 1 (1-2) ^b	1.18 \pm 0.40 1 (1-2) ^b	1.15 \pm 0.38 1 (1-2) ^b	1.23 \pm 0.44 1 (1-2) ^b
Sum of the Radiological Scores		28	2.17 \pm 1.19 2 (1-5) ^a	6.64 \pm 0.67 7 (6-8) ^b	4.83 \pm 0.58 5 (4-6) ^c	5.33 \pm 0.65 5 (4-6) ^c	6.15 \pm 0.90 6 (5-8) ^b	6.31 \pm 1.28 6 (5-9) ^{bc}
		56	3.27 \pm 1.56 3 (2-7) ^a	7.82 \pm 1.25 7 (6-10) ^b	6.55 \pm 1.29 7 (5-9) ^c	6.91 \pm 1.30 7 (5-9) ^{bc}	7.46 \pm 1.66 7 (5-10) ^{bc}	7.38 \pm 1.56 7 (5-10) ^{bc}

^{a,b,c}At each row, different superscript alphabets show significant difference (*P*<0.05)

Table 3: Radiological findings in healing of the bone defects at various postoperative intervals.

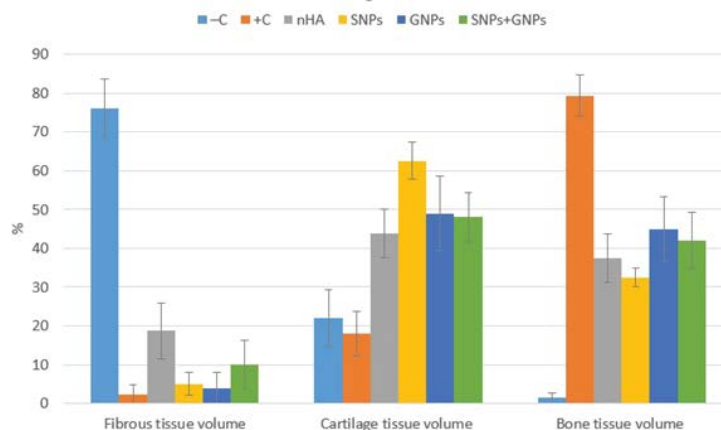


Figure 1: Radiographs at the 1st (a), 28th (b), and 56th (c) postoperative day. The -C are the most radiolucent amongst all groups, whereas +C are the most radiopaque followed by the GNPs, SNPs+GNPs, nHA and SNPs groups at 28 and 56 days after bone surgery. Bone formation was 75-100% at 56 days after bone injury, in the +C group. The nHA and SNPs scaffolds had 50–75% and GNPs and SNPs+GNPs scaffolds had 75-100% bone formation, while it was 0-25% in the -C groups.

the sum of healing scores in comparison to other groups on 28 and 56 days after the injury ($P < 0.05$). The +C group showed significantly the highest proximal bone union compared with other groups on 28 and 56 days after the injury ($P < 0.05$). The best radiological parameters in the treated groups were observed in the GNPs group, followed by GNPs+SNPs, SNPs and nHA groups. The GNPs group had the same values with the +C group in bone formation, distal union, remodeling and sum of healing scores on the 28 and 56 days post-surgery ($P > 0.05$). In comparison among the treated groups, the GNPs showed better bone formation and the sum of healing scores than the nHA ($P = 0.004$ and $P = 0.001$, respectively) and better sum of healing scores than the SNPs group ($P = 0.035$) on the 28th day. The SNPs+GNPs group was comparable to the GNPs and +C groups, but the only significant radiological differences among the treated groups was observed in the sum of healing scores with the nHA group by day 28 after operation ($P = 0.035$). The SNPs group had the same values with the +C group in bone formation and remodeling on the 28 and 56 days, distal union on the 28th day and sum of healing scores on the 56th day ($P > 0.05$). The nHA group had the same values with the +C group only in bone formation on the 56th day, distal union on the 28th and remodeling on the 28th and 56th post-injury days ($P > 0.05$).

Histopathological findings

Histopathological findings were assigned to each group on the basis of the volume of the observed tissues such as the fibrous, fibrocartilage, hyaline cartilage and bone tissues (Table 4 and Figures 2 and 3). At histopathologic level, the lesions in the -C group showed significantly the lowest microscopic scores and had the highest fibrous connective tissue volumes and the lowest bone tissue volumes in comparison to other groups on the 56th day after injury ($P < 0.05$). Then HA, SNPs, GNPs and SNPs+GNPs treated defects had greater cartilage volume compared with the +C group ($P < 0.05$) and the SNPs group also had higher cartilage volume than the -C group ($P = 0.032$). Moreover, all the treated defects had significantly superior microscopic scores than the -C group ($P < 0.05$), but the microscopic score in the SNPs group was also significantly lower than the +C group ($P = 0.016$). The bone volume in all treated groups was significantly superior to the -C group ($P < 0.05$), but they had still lower values compared to the +C group ($P < 0.05$). There were no significant differences in bone volume among the treated groups ($P > 0.05$).

Qualitatively, the gap in the animals of the -C group was replaced with fibrous or fibrocartilages and the lesions showed poor re-vascularization, on 56 days after bone surgery (Figure 2). Bridging callus or histological union did not develop in any of the defects of these animals. These criteria lead to very slow healing process in this group. Both ends of the cortico-medullary implanted autograft were connected to the edges of the old radial bones by a non-homogenous matrix composed of cartilaginous and osseous tissues. A number of

blood vessels were observed in the lesion of this group. The regenerated cartilage and bone spanned the defect and most instantly produced histologic union and the lesions showed some marrow formation.

The defect was filled with a mixed tissue consisting of fibrous connective tissue, fibrocartilage and hyaline cartilage tissue, in the nHA and SNPs treated groups. However, maturation was not as well as those of the +C group. The nHA group had more fibrous connective tissue and less cartilage tissue compared with the SNPs group. The scaffolds in the nHA and SNPs groups were not totally degraded and some remnants were evident in the injured area of the animals in these two groups. The fibrous and cartilage tissues in the defects of the GNPs and SNPs+GNPs groups were almost substituted with bone. The lesions in these animals were mostly filled with fibrocartilage, hyaline cartilage and woven bone particularly in both the distal and proximal ends of the defects and maturation was almost near to those of the +C group. No remnants of the scaffold were seen in the injured area of the GNPs and SNPs+GNPs groups. Both the GNPs and SNPs+GNPs groups showed hypertrophic bone edges and the newly formed cells were proliferating from the bone edges into the middle part of the defect area and more woven bone formation was seen in the lesions of these groups. In most cases, such feature was less evident in the injured areas of the nHA and SNPs groups. In general, some inflammatory response was evident in the lesions of the animals of different treatment groups at the 56th post injury day, particularly in the lesion of those groups that the scaffolds remnants were still persisted.

Scanning electron microscopy

Irregular collagen fibrils were seen in the defects of -C group after 56 days of bone injury (Figure 4). An accumulation of hydroxyapatite crystals was visible along with the newly formed bone, in the lesions of the +C group. Calcified cartilaginous matrices containing a number of deposited hydroxyapatite crystals were observed as the newly regenerated tissue in the treated nHA, SNPs, GNPs and SNPs+GNPs lesions.

Biomechanical performance

The data obtained from the biomechanical testing have been shown in Table 5. The failure mechanism of the bones was very consistent; the failure took place exactly at the defected area with the fracture line being perpendicular to the long axis of the bone. There were statistically significant differences in terms of ultimate and yield strength between the -C group with the GNPs ($P = 0.012$ and $P = 0.012$, respectively) and the SNPs+GNPs ($P = 0.020$ and $P = 0.036$, respectively) groups. Not only there were no significant differences in these parameters in the nHA and SNPs groups, compared with the -C group, but the yield strength in both groups ($P = 0.010$ and $P = 0.014$, respectively) and ultimate strength in SNPs group ($P = 0.026$) were also significantly lower than the +C group. The GNPs group was the only group that had significantly

	Mean \pm SD Median (min-max)					
	Control		Treatment			
	-C (n=5)	+C (n=5)	nHA (n=5)	SNPs (n=5)	GNPs (n=5)	SNPs+GNPs (n=5)
Emery's Score	2.20 \pm 0.45	6.20 \pm 0.45	4.75 \pm 1.26	4.50 \pm 1.00	5.60 \pm 0.55	5.20 \pm 1.30
	2 (2-3) ^c	6 (6-7)	5 (3-6) ^a	5 (3-5) ^{a,A}	6 (5-6) ^b	6 (3-6) ^b

^c $P < 0.05$ (compared with the +C, nHA, SNPs, GNPs and SNPs+GNPs by Manne-Whitney U test)

^a $P = 0.016$ (compared with the -C by Manne-Whitney U test)

^b $P = 0.008$ (compared with the -C by Manne-Whitney U test)

^A $P = 0.016$ (compared with the +C by Manne-Whitney U test)

Table 4: Histopathological scores for healing of bone defects after 56 days of injury.

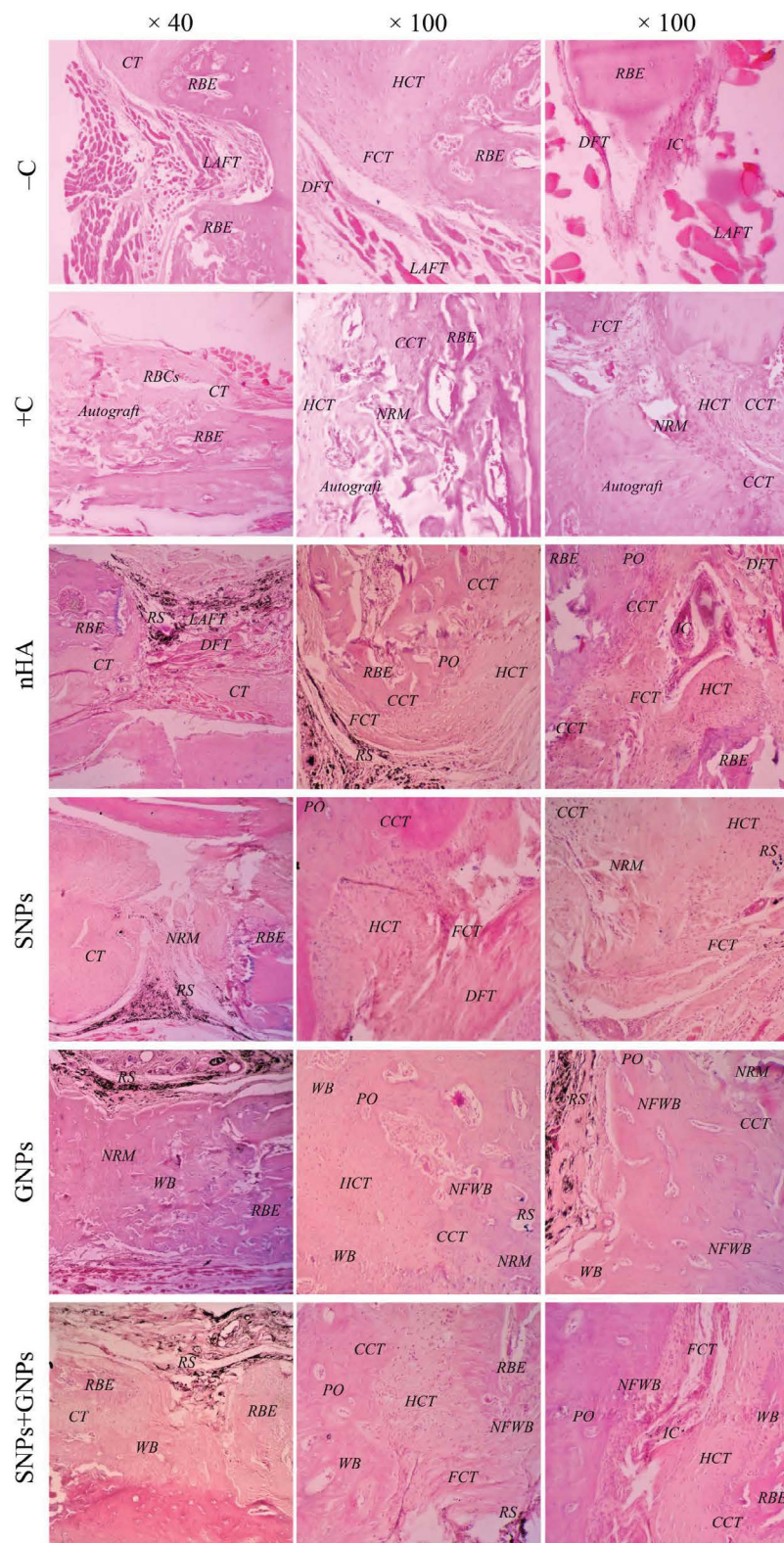


Figure 2: Tissue volumes of the healing bone defects after 56 days of bone injury. The volume of fibrous tissue in the -C group was significantly higher ($P < 0.05$) and the volume of bone tissue was significantly lower ($P < 0.05$) than the other groups. The nHA, SNPs, GNPs and SNPs+GNPs groups showed significantly higher volume of cartilage tissue when compared to the +C groups ($P = 0.032$, $P = 0.016$, $P = 0.032$, $P = 0.016$, respectively). The SNPs group also had greater cartilage tissue than the -C group ($P = 0.032$). The bone tissue volume of all the treated groups was significantly superior to the -C group ($P < 0.05$), but they had still lower values compared to the +C group ($P < 0.05$).

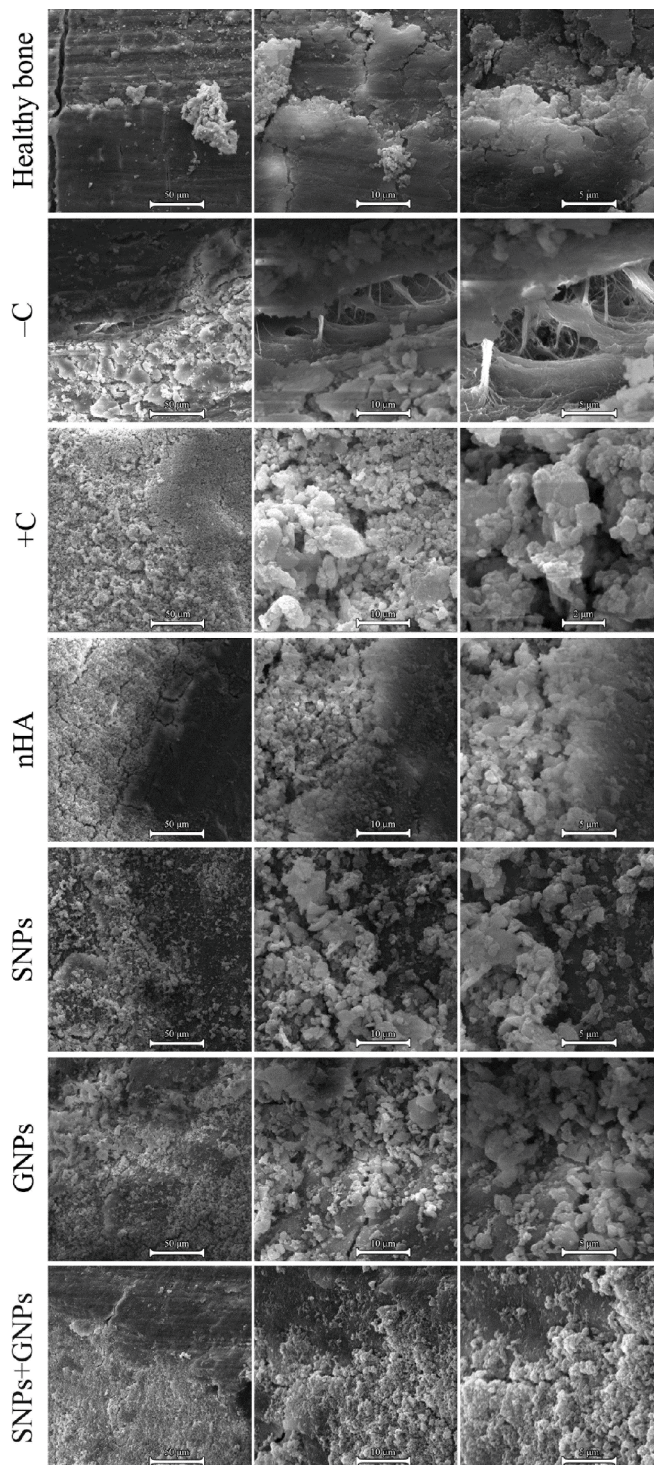


Figure 3: Histopathological sections of the radial bone defects after 56 days of injury; stained with H & E, longitudinal view. The lesion has been filled with a loose areolar connective tissue in the -C group and a fibrocartilage tissue was visible at the edges of the radial bone of the defects in the animals of this group. Note the mild inflammatory response consisting of mononuclear cells in the defected area of this group. In the +C group, a matrix composed of hyaline cartilage, calcified cartilage and osseous tissue are predominant in the defect site. Note the neovascularization in the grafted area of this group. The defects in the nHA and SNPs group are filled with a non-homogenous matrix composed of fibrous connective tissue, fibrocartilage and hyaline cartilage. A hyaline cartilaginous matrix at the middle part of the lesion and calcified cartilage at the edges of the lesion have filled the defected site in the nHA and SNPs groups. In the injured area of both the GNPs and SNPs+GNPs groups the newly formed cells are proliferating from the bone edges into the middle part of the defect area and more woven bone formation are seen in the lesions of the animals of these groups. Note extensive development of the woven bone containing several osteons at the bone edges in these two groups.
 RBE: Radial Bone Edge; LAFT: Loose Areolar Fibrous Tissue; CT: Cartilaginous Tissue; DFT: Dense Fibrous Tissue; HCT: Hyaline Cartilaginous Tissue; FCT: Fibrocartilaginous Tissue; IC: Inflammatory Cells; RBCs: Red Blood Cells; NRM: Newly Regenerated Matrix; CCT: Calcified Cartilaginous Tissue; WB: Woven Bone; PO: Primary Osteon; RS: Remnants of Scaffold; NFWB: Newly Formed Woven Bone

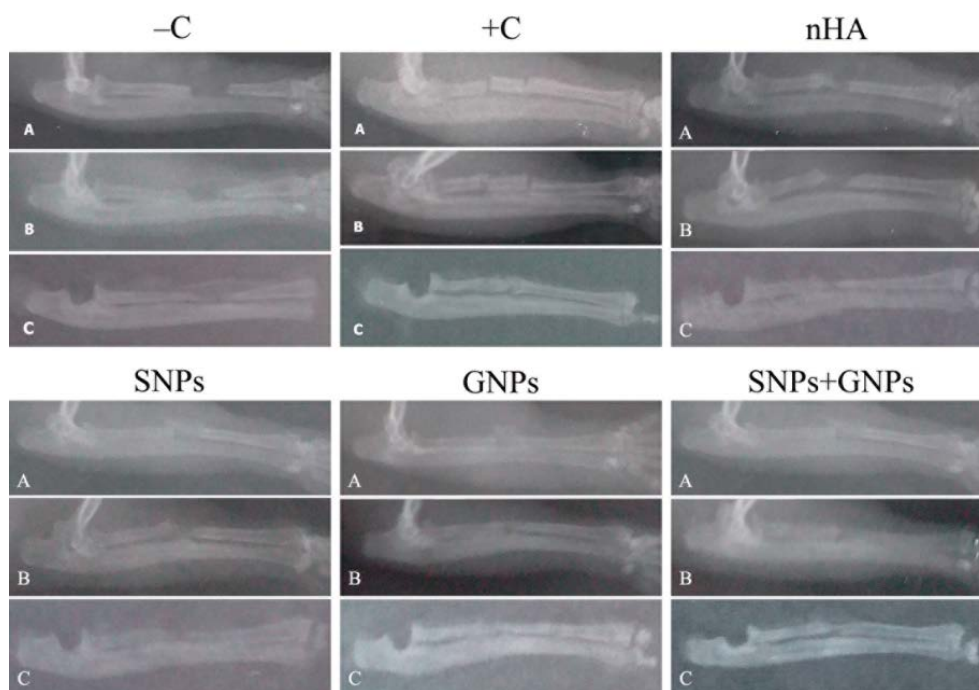


Figure 4 Scanning ultramicrographs of the bones after 56 days of surgery. Highly calcified bone matrix can be seen in the healthy bone. The defect has been filled with collagen fibrils in the -C group. Calcified bone matrix and hydroxyapatite crystals has filled the defect sites in the +C group. A calcified cartilage tissue and calcified bone matrix containing deposited hydroxyapatite crystals are present in the defect sites in the nHA, SNPs, GNPs and SNPs+GNPs groups.

Three Point Bending Test Criteria	Mean ± SEM					
	Control		Treatment			
	-C (n=5)	+C (n=5)	nHA (n=5)	SNPs (n=5)	GNPs (n=5)	SNPs+GNPs (n=5)
Ultimate strength (N)	18.08 ± 1.69	31.18 ± 0.80 [*]	22.92 ± 1.88	21.98 ± 2.00 ^A	28.20 ± 2.29 ^a	27.54 ± 2.40 ^b
Yield strength (N)	14.36 ± 1.25	28.23 ± 0.61 [*]	18.12 ± 2.26 ^B	18.46 ± 2.26 ^C	24.36 ± 2.33 ^c	23.02 ± 1.97 ^d
Stiffness (N/mm)	16.76 ± 2.37	30.99 ± 1.70	29.24 ± 2.71	30.97 ± 3.41	38.40 ± 6.84 ^e	31.37 ± 2.97
Strain (%)	7.43 ± 0.35	6.99 ± 0.62	7.09 ± 0.91	7.09 ± 0.43	5.73 ± 0.61	6.01 ± 0.50
Energy absorption (N.mm)	20.20 ± 2.74	37.07 ± 1.90 [*]	26.81 ± 5.79	21.56 ± 3.34 ^D	31.50 ± 3.82	25.17 ± 1.47

^{*}P<0.05 (compared with the -C by one-way ANOVA test)
^AP=0.026(compared with the +C by one-way ANOVA test)
^BP=0.010 (compared with the +C by one-way ANOVA test)
^CP=0.014 (compared with the +C by one-way ANOVA test)
^DP=0.044 (compared with the +C by one-way ANOVA test)
^aP=0.012 (compared with the -C by one-way ANOVA test)
^bP=0.020 (compared with the -C by one-way ANOVA test)
^cP=0.012 (compared with the -C by one-way ANOVA test)
^dP=0.036 (compared with the -C by one-way ANOVA test)
^eP=0.005 (compared with the -C by one-way ANOVA test)

Table 5: Biomechanical findings at the 56th postoperative day.

superior stiffness compared to the -C group (P=0.005). There were no statistically significant differences between the four treatment groups with those of the +C and -C groups in terms of strain (P<0.05). The energy absorption in all treatment groups was in a lower level than the +C group but this difference was only significant in the SNPs group (P=0.044).

Discussion

In recent years, the search for a substitute to autograft in large bone defects has focused on composite from advanced biomaterials [7,33]. Nanostructural materials have proven to be excellent candidates for

implantable scaffolds to promote higher cellular differentiation and proliferation [2,34]. The primary properties that these nanomaterials must have to be successfully applied in biomedicine are good biocompatibility, high stability in biological environments, high ability to allow cells to proliferate and differentiate and low toxicity [2].

To evaluate the bone healing potential of the SNPs, GNPs and their combinations a defect model was established in the radial bone of rat. This model has previously been reported suitable because there is no need for internal or external fixation which influences the healing process [19,35]. The defect was made in the middle portion of the radius as long as 5 mm to induce a nonunion defect as a critical size defect and

to prevent spontaneous and rapid healing [19,36]. The hypothesis was on the basis that both the SNPs and GNPs may have some useful effects on bone regeneration but each of such biomaterials may have different potency. In addition, combination of these biomaterials may keep the useful effects of both biomaterials, while this strategy may reduce the limitations of the individuals.

The results of the radiological, histological, ultrastructural and biomechanical analysis showed that regardless of the +C (autograft) group, among the scaffolds used in this investigation, the best results were obtained from the GNPs treated defects followed by SNPs+GNPs. When compared to other treatments groups, the bone defects treated with SNPs followed by nHA were associated with lower healing and the differences between them and the +C group were significant in most radiological, histopathological and biomechanical parameters. In fact, the healing process in the -C (empty defect) group remained in the initial stages of healing and fibrous connective tissue was the main constituent in the lesions of the animals of this group, while the healing stage was more advanced in the SNPs and nHA treated group and there was some evidence of cartilage and bone cells in these groups. The GNPs and SNPs+GNPs showed significant bone regeneration with more new bone formation.

The broad antimicrobial features of silver are well known and also bone composite has already been loaded with silver [9]. Although a huge background exists in the literature that have suggested application of SNPs as an acceptable biomaterial in bone tissue engineering [1,10,11], here we showed that its potential in promoting bone healing was inferior to the autograft and GNPs. This is a fact that the *in vitro* characterizations and results such as MTT and LDH assay and cell differentiation tests do not guarantee the real *in vivo* role of the composite [12,19]. Therefore, our *in vivo* results did not confirm the *in vitro* results of the formerly published researches. We showed that both the SNPs and nHA scaffolds have some osteoinductive properties because in both groups some evidences of new bone formation were seen after 56 days of injury. However, new bone formation was limited to both defect edges and these scaffolds were not able to induce bone formation in the middle of the defect area and thus, they displayed low osteoconductive properties.

In bone tissue engineering, GNPs are noteworthy materials because of their potential influence in bone tissue regeneration [12]. The effects of GNPs as osteogenic agents have well been described, in the previous studies [2,15,16]. However, the previous researches just confirmed its osteogenic effects at *in vitro* condition. Although the effects of GNPs in the osteogenic differentiation are evident at *in vitro*, the interactions between GNPs and bone tissues have not been investigated. The results of *in vitro* researches may not always be the same as those of the *in vivo* ones [12,19]. Therefore, it was necessary to investigate the osteogenic effects of GNPs at *in vivo* condition. Here, we have presented that bone formation, remodeling, distal union and the biomechanical performances such as the ultimate strength, yield strength and stiffness, in the GNPs treated defects were statistically comparable to those treated by the autograft. The present experiment also showed that SNPs demonstrated a more positive effect in bone regeneration when it was combined with GNPs. The SNPs+GNPs composite had similar radiological, histopathological and biomechanical parameters with the GNPs composite and except for the stiffness all these parameters were statistically similar to the +C group. These criteria might be attributed to the higher biocompatible and bioactive properties of the GNPs than the SNPs and thus the GNPs improved the effectiveness of the SNPs.

We confirmed that nHA and SNPs could induce bone formation in

the margins of the defect areas, while GNPs and SNPs+GNPs conducted tissue regeneration towards the central part of the defect area. The calcification process of cortical bone can expose osteoinductive growth factors within the HA mineralized matrix. On the other hand, the collagenous framework of the Gel/FPG may be responsible for its osteoconductive properties [37,38]. Given these findings, the GNPs composite materials could find excellent possible applications as scaffold for various bone defects to increase bone regeneration. In line with our findings, Heo et al. [12] showed that hydrogels loaded with a high concentration of GNPs have significant effects on new bone formation and can be beneficial materials in bone tissue engineering.

Embedment of inorganic nanoparticles into polymeric Gel is an effective procedure in enhancing the functionality of the nanoparticles in biological systems [12]. Therefore, combination of the Gel+nHA and SNPs+GNPs results in formation of multifunctional nanocomposites possessing major potential in nanomedicine. Moreover, presence of Gel structures that can be easily used with various biomolecules, proteins, drugs, FPG and particularly the growth factors give these materials great potential in development of novel functional scaffolds in cell biology to increase bone formation potential. These structures have been found to possess proper biocompatibility to proliferate the bone cells. Such complex nanostructural systems could be the foundation in formation of highly active scaffolds in tissue and bone regeneration. Gel as a good cell adhesiveness vehicle can evoke the mesenchymal and osteochondral progenitor cells into the defect site [29,39,40], while FPG as a reservoir of critical GFs can promote cell proliferation, cell differentiation and matrix synthesis [41-43]. It has been shown that coating of the SNPs and GNPs bone cements with blood or blood components not only did not weaken or impaired their antibacterial effects but also slightly increased the antibacterial activities and proved its suitability for clinical use [9,44,45]. A scientific explanation for this observation does not exist as yet. Coating of the SNPs and GNPs surfaces with blood product was done to mimic the clinical situation in surgery where bone cement is immediately covered with blood when placed into bone defect [9].

Based on the results of the present study and regarding the formerly published results from the *in vitro* and *in vivo* researches, it seems SNPs and GNPs have different behavior on bone regeneration. The GNPs showed significant bone regeneration with more new bone formation in the central part of the defect area, while, the SNPs exhibited only partial bone regeneration with more new bone formation in the margins of the bone defect.

Conclusion

In conclusion, this study confirmed the failure of spontaneous bone healing in the critical sized radial bone defects in rats. Furthermore, the nHA and SNPs alone significantly affect bone healing and regeneration; however, the treated defects were structurally and functionally inferior to those of the autograft. The GNPs and SNPs+GNPs promoted new bone formation more than that of the untreated defects and also closely comparable with those of the autograft group. Although all the scaffolds had some beneficial effectiveness in bone regeneration, the GNPs-containing scaffolds, similar to the autograft treated group, effectively increased the proliferation and differentiation of osteoblasts and osteocytes, facilitated osteoinduction and was more effective in improving the structural and functional characteristics of the newly formed bone in comparison to other treatment groups. This study clearly indicated that GNPs have a high biocompatibility with the bone tissue and could be the foundation for multifunctional technologies in the bone and tissue regeneration field.

Acknowledgement

The authors would like to thank the authorities of Shiraz University for their kind cooperation. This work was partially supported by the Shiraz University Foundation, Shiraz, Iran. We would also thank the INSF (grant number 96006039) for its financial support. The funders had no role in the study design, data collection and analysis, decision to publish or preparation of the manuscript. Prof. Oryan A, Prof. Meimandi-Parizi AH and Dr. Gholipour H were involved in all study procedures such as study design, data collections, data analysis and writing.

References

1. Saravanan S, Nethala S, Pattnaik S, Tripathi A, Moorthi A, et al. (2011) Preparation, characterization and antimicrobial activity of a bio-composite scaffold containing chitosan/nano-hydroxyapatite/nano-silver for bone tissue engineering. *Int J Biol Macromol* 49: 188-193.
2. Biris AR, Mahmood M, Lazar MD, Dervishi E, Watanabe F, et al. (2011) Novel multicomponent and biocompatible nanocomposite materials based on few-layer graphenes synthesized on a gold/hydroxyapatite catalytic system with applications in bone regeneration. *J Phys Chem C* 115: 18967-18976.
3. Takahashi Y, Yamamoto M, Tabata Y (2005) Enhanced osteoinduction by controlled release of bone morphogenetic protein-2 from biodegradable sponge composed of gelatin and β -tricalcium phosphate. *Biomaterials* 26: 4856-4865.
4. Kim HW, Knowles JC, Kim HE (2005) Hydroxyapatite and gelatin composite foams processed via novel freeze-drying and crosslinking for use as temporary hard tissue scaffolds. *J Biomed Mater Res A* 72: 136-145.
5. Peter M, Ganesh N, Selvamurugan N, Nair S, Furuie T, et al. (2010) Preparation and characterization of chitosan-gelatin/nanohydroxyapatite composite scaffolds for tissue engineering applications. *Carbohydr Polym* 80: 687-694.
6. Liu Y, Lu Y, Tian X, Cui G, Zhao Y, et al. (2009) Segmental bone regeneration using an rhBMP-2-loaded gelatin/nanohydroxyapatite/fibrin scaffold in a rabbit model. *Biomaterials* 30: 6276-6285.
7. Khan MN, Islam JM, Khan MA (2012) Fabrication and characterization of gelatin-based biocompatible porous composite scaffold for bone tissue engineering. *J Biomed Mater Res A* 100: 3020-3028.
8. Singh R, Nalwa HS (2011) Medical applications of nanoparticles in biological imaging, cell labeling, antimicrobial agents and anticancer nanodrugs. *J Biomed Nanotechnol* 7: 489-503.
9. Alt V, Bechert T, Steinrücke P, Wagener M, Seidel P, et al. (2004) An *in vitro* assessment of the antibacterial properties and cytotoxicity of nanoparticulate silver bone cement. *Biomaterials* 25: 4383-91.
10. Yazdimaghani M, Vashae D, Assefa S, Walker K, Madhally S, et al. (2014) Hybrid macroporous gelatin/bioactive-glass/nanosilver scaffolds with controlled degradation behavior and antimicrobial activity for bone tissue engineering. *J Biomed Nanotechnol* 10: 911-931.
11. Wiglusz RJ, Kedziora A, Lukowiak A, Doroszkiewicz W, Strek W (2012) Hydroxyapatites and europium (III) doped hydroxyapatites as a carrier of silver nanoparticles and their antimicrobial activity. *J Biomed Nanotechnol* 8: 605-612.
12. Heo DN, Ko W-K, Bae MS, Lee JB, Lee D-W, et al. (2014) Enhanced bone regeneration with a gold nanoparticle-hydrogel complex. *J Mater Chem B* 2: 1584-1593.
13. Giljohann DA, Seferos DS, Daniel WL, Massich MD, Patel PC, et al. (2010) Gold nanoparticles for biology and medicine. *Angew Chem Int Ed* 49: 3280-3294.
14. Dykman L, Khlebtsov N (2012) Gold nanoparticles in biomedical applications: Recent advances and perspectives. *Chem Soc Rev* 41: 2256-2282.
15. Yi C, Liu D, Fong C-C, Zhang J, Yang M (2010) Gold nanoparticles promote osteogenic differentiation of mesenchymal stem cells through p38 MAPK pathway. *ACS Nano* 4: 6439-6448.
16. Liu D, Zhang J, Yi C, Yang M (2010) The effects of gold nanoparticles on the proliferation, differentiation, and mineralization function of MC3T3-E1 cells *in vitro*. *Sci Bull* 55: 1013-1019.
17. Kim K, Fisher JP (2007) Nanoparticle technology in bone tissue engineering. *J Drug Target* 15: 241-252.
18. NRC (2011) Guide for the care and use of laboratory animals. 8th edn. National Academies Press, Washington (DC).
19. Oryan A, Alidadi S, Bigham-Sadegh A, Moshiri A (2016) Comparative study on the role of gelatin, chitosan and their combination as tissue engineered scaffolds on healing and regeneration of critical sized bone defects: An *in vivo* study. *J Mater Sci Mater Med* 27: 155.
20. Thom J, Sørensen H, Weis-Fogh U, Andersen M (2004) Autologous fibrin glue with growth factors in reconstructive maxillofacial surgery. *Int J Oral Maxillofac Surg* 33: 95-100.
21. Butterfield KJ, Bennett J, Gronowicz G, Adams D (2005) Effect of platelet-rich plasma with autogenous bone graft for maxillary sinus augmentation in a rabbit model. *J Oral Maxillofac Surg* 63: 370-376.
22. Findikcioglu K, Findikcioglu F, Yavuzer R, Elmas C, Atabay K (2009) Effect of platelet-rich plasma and fibrin glue on healing of critical-size calvarial bone defects. *J Craniofac Surg* 20: 34-40.
23. Lane JM, Sandhu H (1987) Current approaches to experimental bone grafting. *Orthop Clin North* 18: 213-225.
24. Oryan A, Bigham-Sadegh A, Abbasi-Teshnizi F (2014) Effects of osteogenic medium on healing of the experimental critical bone defect in a rabbit model. *Bone* 63: 53-60.
25. Parizi AM, Oryan A, Shafiei-Sarvestani Z, Bigham-Sadegh A (2013) Effectiveness of synthetic hydroxyapatite versus Persian Gulf coral in an animal model of long bone defect reconstruction. *J Orthop Trauma* 14: 259-268.
26. Shafiei-Sarvestani Z, Oryan A, Bigham AS, Meimandi-Parizi A (2012) The effect of hydroxyapatite-hPRP and coral-hPRP on bone healing in rabbits: radiological, biomechanical, macroscopic and histopathologic evaluation. *Int J Surg* 10: 96-101.
27. Emery SE, Brazinski MS, Koka A, Bensusan JS, Stevenson S (1994) The biological and biomechanical effects of irradiation on anterior spinal bone grafts in a canine model. *J Bone Joint Surg Am* 76: 540-548.
28. Bigham-Sadegh A, Oryan A, Mirshokraei P, Shadkhist M, Basiri E (2013) Bone tissue engineering with periosteal-free graft and pedicle omentum. *ANZ J Surg* 83: 255-261.
29. Moshiri A, Shahrezaee M, Shekarchi B, Oryan A, Azma K (2015) Three-dimensional porous gelatin-simvastatin scaffolds promoted bone defect healing in rabbits. *Calcif Tissue Int* 96: 552-564.
30. Leppänen O, Sievänen H, Jokihaara J, Pajamäki I, Järvinen TL (2006) Three-point bending of rat femur in the mediolateral direction: Introduction and validation of a novel biomechanical testing protocol. *J Bone Miner Res* 21: 1231-1237.
31. Järvinen T, Sievänen H, Kannus P, Järvinen M (1998) Dual-energy X-ray absorptiometry in predicting mechanical characteristics of rat femur. *Bone* 22: 551-558.
32. Oryan A, Parizi AM, Shafiei-Sarvestani Z, Bigham A (2012) Effects of combined hydroxyapatite and human platelet rich plasma on bone healing in rabbit model: radiological, macroscopic, histopathological and biomechanical evaluation. *Cell Tissue Bank* 13: 639-651.
33. Trouillas M, Prat M, Doucet C, Ernou I, Laplace-Builhé C, et al. (2013) A new platelet cryoprecipitate glue promoting bone formation after ectopic mesenchymal stromal cell-loaded biomaterial implantation in nude mice. *Stem Cell Res Ther* 4: 1.
34. Zanello LP, Zhao B, Hu H, Haddon RC (2006) Bone cell proliferation on carbon nanotubes. *Nano Lett* 6: 562-567.
35. An YH, Freidman RJ (1998) Animal models in orthopaedic research. CRC Press,
36. Öztürk A, Yetkin H, Memis L, Cila E, Bolukbasi S, et al. (2006) Demineralized bone matrix and hydroxyapatite/tri-calcium phosphate mixture for bone healing in rats. *Int Orthop* 30: 147-152.
37. Bigham A, Dehghani S, Shafiei Z, Nezhad ST (2009) Experimental bone defect healing with xenogenic demineralized bone matrix and bovine fetal growth plate as a new xenograft: radiological, histopathological and biomechanical evaluation. *Cell Tissue Bank* 10: 33-41.
38. Meimandi PA, Oryan A, Haddadi S, Bigham SA (2014) Histopathological and biomechanical evaluation of bone healing properties of DBM and DBM-G90 in a rabbit model. *Acta Orthop Traumatol Turc* 49: 683-689.
39. Kakkar P, Verma S, Manjubala I, Madhan B (2014) Development of keratin-chitosan-gelatin composite scaffold for soft tissue engineering. *Mater Sci Eng C* 45: 343-47.

-
40. Zhang S, Huang Y, Yang X, Mei F, Ma Q, et al. (2009) Gelatin nanofibrous membrane fabricated by electrospinning of aqueous gelatin solution for guided tissue regeneration. *J Biomed Mater Res A* 90: 671-679.
41. Zhu S-J, Choi B-H, Jung J-H, Lee S-H, Huh J-Y, et al. (2006) A comparative histologic analysis of tissue-engineered bone using platelet-rich plasma and platelet-enriched fibrin glue. *Oral Surg Oral Med Oral Pathol Oral Radiol Endod* 102: 175-179.
42. Burnouf T, Goubran HA, Chen T-M, Ou K-L, El-Ekiaby M, et al. (2013) Blood-derived biomaterials and platelet growth factors in regenerative medicine. *Blood Rev* 27: 77-89.
43. Burnouf T, Su CY, Radosevich M, Goubran H, El-Ekiaby M (2009) Blood-derived biomaterials: Fibrin sealant, platelet gel and platelet fibrin glue. *ISBT Sci Ser* 4: 136-142.
44. Bechert T, Steinrücke P, Guggenbichler J-P (2000) A new method for screening anti-infective biomaterials. *Nat Med* 6: 1053-1056.
45. Böswald M, Lugauer S, Regenfus A, Greil J, Guggenbichler JP (1999) The Erlanger silver catheter: *In vitro* results for antimicrobial activity. *Infection* 27: S24-S29.